

# ISI Web of Knowledge<sup>SM</sup>

## Journal Citation Reports<sup>®</sup>

WELCOME HELP

2012 JCR Science Edition

### Journal Summary List

[Journal Title Changes](#)

Journals from: search ISSN for '0921-0296'

Sorted by:

Journals 1 - 1 (of 1)

Navigation icons: first, previous, [ 1 ], next, last

Page 1 of 1

Ranking is based on your journal and sort selections.

| Mark                     | Rank | Abbreviated Journal Title<br><i>(linked to journal information)</i> | ISSN      | JCR Data    |               |                      |                 |          |                 | Eigenfactor <sup>®</sup> Metrics |                                      |
|--------------------------|------|---|-----------|-------------|---------------|----------------------|-----------------|----------|-----------------|----------------------------------|--------------------------------------|
|                          |      |   |           | Total Cites | Impact Factor | 5-Year Impact Factor | Immediacy Index | Articles | Cited Half-life | Eigenfactor <sup>®</sup> Score   | Article Influence <sup>®</sup> Score |
| <input type="checkbox"/> | 1    | <a href="#">J INTELL ROBOT SYST</a>                                 | 0921-0296 | 775         | 0.827         | 0.965                | 0.111           | 108      | 5.8             | 0.00273                          | 0.387                                |

Journals 1 - 1 (of 1)

Navigation icons: first, previous, [ 1 ], next, last

Page 1 of 1

[Acceptable Use Policy](#)  
Copyright © 2014 Thomson Reuters.



# HTG-Based Kinematic Modeling for Positioning of a Multi-Articulated Wheeled Mobile Manipulator

L. A. Zúñiga-Avilés · J. C. Pedraza-Ortega ·  
E. Gorrostieta-Hurtado · S. Tovar-Arriaga ·  
J. M. Ramos-Arreguín · M. A. Aceves-Fernández ·  
J. E. Vargas-Soto

Received: 10 July 2013 / Accepted: 26 January 2014  
© Springer Science+Business Media Dordrecht 2014

**Abstract** This paper presents a novel methodology for positioning an explosive ordnance device (EOD) which consists of a mobile manipulator with 12° of freedom. The approach uses an extension of a homogeneous transformation graph (HTG) which can be used in the kinematic modeling of mobile manipulators and unmanned aerial vehicles. In this approach the complete kinematics is modeled as one unit in contrast to previous approaches where the manipulator and mobile body are decoupled. The system is tested in several escenarios (simulated and real experimentation) like approaching to an explosive device location on the plane as well as in slope ways, climbing stairs, lifting itself and manipulating procedures. All the aforementioned scenarios were developed using the HTG which establishes the appropriate transformations and interaction parameters of the coupled system. Finally, the system is tested (simulated and

real experimentation) for positioning its end device in a target with a RMS positioning average error of 7.91 mm which is acceptable for this kind of devices.

**Keywords** Extended homogenous transform graph · Explosive ordnances devices · Mobile-manipulator locomotion

## 1 Introduction

A mobile manipulator is rigid robotic manipulator mounted atop of a wheeled mobile platform. In comparison to fixed-base manipulators, such a combined system is able to perform manipulation tasks in larger areas with high versatility. Therefore, mobile manipulators are useful in handling dangerous devices which are often called explosives ordnance devices (EOD). Those devices are used by many national forces around the world [1, 2]. The modular robot concept could be traced back to the 1970's [3]. Nevertheless, these kinds of robots are normally designed for tele-operated tasks [4–6].

When the base is a wheeled platform subject to nonholonomic constraints, the robot is referred to as a nonholonomic mobile manipulator. Several publications have been made about locomotion of mobile manipulators, being Yamamoto's work the most cited [7]. Mazur and Bayle et al. have written several papers in relation to control strategies and path following [8–10].

---

L. A. Zúñiga-Avilés  
Centro de Ingeniería y Desarrollo Industrial (CIDESI),  
Av. Playa Pie de la Cuesta 702, Desarrollo San Pablo, 76130  
Querétaro Qro., México

J. C. Pedraza-Ortega · E. Gorrostieta-Hurtado ·  
S. Tovar-Arriaga (✉) · J. M. Ramos-Arreguín ·  
M. A. Aceves-Fernández · J. E. Vargas-Soto  
CIDIT-Facultad de Informática,  
Universidad Autónoma de Querétaro,  
Av. de las Ciencias S/N, Juriquilla,  
76230 Querétaro Qro., México  
e-mail: saulotov@yahoo.com.mx

It is only until 1988 where the dynamic behavior of mobile manipulators, was considered [11]. In 1989, Wiens [12] studied dynamic coupling between a planar vehicle and a one-link manipulator on the vehicle. Further works include dynamic model of some specific type [13–15]. Reactive motion has been studied for mobile manipulators in the case of omnidirectional wheeled platforms using a dynamical model [16]. In [17] Li et al. develop a reduced model for mobile manipulators such that Markovian theory can be used to model the fault tolerant considering a more realistic element-wise way to describe the transition-rate uncertainty.

Building up the dynamic model of a nonholonomic mobile modular manipulator is a challenging task due to the interactive motions between the modular manipulator and the mobile platform, as well as the nonholonomic constraints of the mobile platform [18]. Also a trajectory following becomes even more complex and difficult to achieve.

Published works, focused on control, kinematic redundancy, tracking trajectories and manipulability [8, 19–21], are mainly about mobile planar manipulator (not considering the load and operation cases) where the manipulator and the mobile dynamics are taken into account separately. Advanced studies have been carried out for controlling multiple robot manipulators grasping a common object which are robust to external disturbances [22, 23]. In [24] effective adaptive robust-control strategies were presented to address the force/motion control of holonomic-constrained nonholonomic mobile manipulators in the presence of uncertainties and disturbances.

HTG is the abbreviation of Homogeneous Transformation Graph introduced by Paul R.P. [25] for fixed manipulators. The HTG, published in our previous works [26–29], contemplate systems about global coordinates, local coordinates and base coordinates of manipulators, which allows to use such a diagram in UAV's, mobile manipulators and other systems that consider complex manipulators, including objects that are attached to the end effector. In the present work, a kinematic interaction table was developed that allows to formulate a diagram that considers the base coordinates of the manipulators about the local coordinates of a mobile platform in relation to the global coordinates.

This paper shows the development of a modeling methodology for mobile manipulators applied in

the mechatronic design of a multi-articulated wheeled mobile robot manipulator called MMR12-EOD. This robot will be used in tasks like positioning, handling and transporting of explosive devices. Due to its configuration, the robot is capable to do complex movements like climbing stairs or moving along terrains full of obstacles. One characteristic of our system is that the complete kinematic is modeled as one unit in contrast to previous works where the manipulator and mobile body are decoupled.

## 2 Methodology

In this section, a modeling methodology for wheeled mobile manipulators is presented. This methodology is organized in the following steps: preliminary analysis, master map, position and orientation diagram, homogenous transformation graph (HTG), kinematics schemes of operation scenarios, kinematics interactions, forward and inverse kinematic, constraints, dynamic parameters.

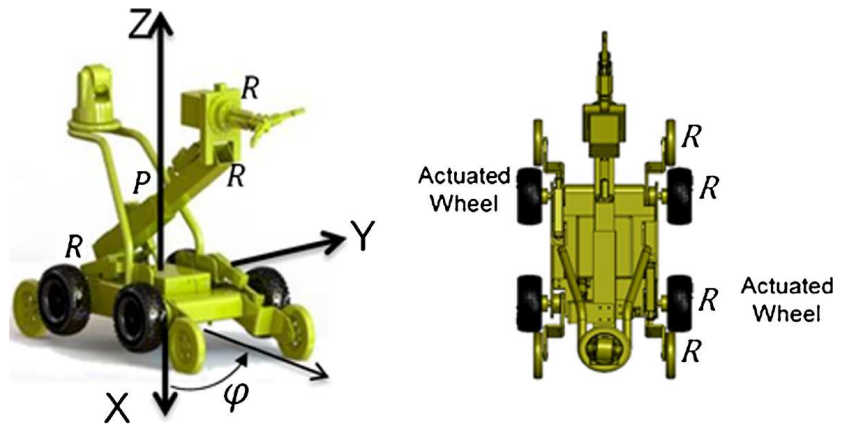
### 2.1 Preliminary Analysis

The MMR12-EOD robot is capable of doing locomotion on different types of surfaces by means of its action wheels. The wheels must be mounted on devices that allow relative motion between their guiding point and the surface (it has one rolling contact point) [30]. These characteristics allow modeling the system, but the slippage of the wheels makes it difficult due to the error presented in the robot autolocation. Figure 1 shows that the mobile platform has 4 dof, the manipulator has 4 dof and the added subsystem has 4.

The requirements of the MMR12-EOD robot are: average velocity of 0.5 m/s and requires supporting a load of 10 kg at its end effector.

The system contains different kinds of sensors which are: absolute encoder that measures the displacement angle of joint 1. Two inductive sensors used to measure the height of link 2 in its minimum and maximum extension. Proximity sensor that measures the operation range of prismatic joint 2. Two absolute encoders for joint 3 and 4, one each. Six absolute encoders sen-cos in each servomotor of the actuated wheels and four more in each lifting arm.

**Fig. 1** MMR12-EOD robot. **a** Isometric view (shows the rotation angle around the local coordinates), **b** top view showing the alternate actuated wheels



## 2.2 Master Map

The master map is a diagram that shows an overview of the model development, from which its subsystems and homogenous transformations are identified. First, the external and internal constraints are shown, being the first of them related to considered surface for the localization of the local coordinates in reference to the global coordinates. The internal restrictions are proposed according to the nonholonomic features of the mobile platform. Then, the scheme is classified with the nomenclature M-MMR-“add-subsystem”, where M is the manipulator, MMR is the mobile body and any other add-subsystem, like a robotic arm. In case that another subsystem is added to the system, e.g. a second manipulator, the homogeneous transformation will be referenced to the local coordinates “C”. The master map has stages regarding to subsystems for conventional mobile manipulators in relation to the orientation, approaching and manipulation tasks, in this case the mobile manipulator has an added subsystem formed by 2 coupled lifting arms, which will be considered for lifting and climbing tasks.

In order to model the MMR12-EOD robot, 7 stages are considered in 5 real operation scenarios, in which the assessment of behavior from the full system with load and without load are included. For this robot, the stages are as follows:

- The added subsystem is considered in neutral position and in operation, related to the local coordinate “C”. The added subsystem is called “A” in the master map. This stage is neglected if the manipulator does not have any added subsystem.
- The manipulator uses just its degrees of freedom to do tracking trajectories tests, in relation to the

“0” coordinate (origin), which is located on the manipulator’s base.

- The mobile platform is moved forward with the mounted manipulator and does a tracking trajectory test, from coordinate “C” to global coordinate “G<sup>4</sup>”.
- Considering the coupled system without advance of the mobile platform, the manipulator do the tracking trajectories test, assuming that the mobile platform rotates about its axis, in relation to the local coordinate “C”.
- The mobile platform is moved forward coupled with the manipulator and does a tracking trajectory test, from “C” coordinate to the “G<sup>4</sup>” global coordinate.
- The coupled system is moved following a straight line and its manipulator is moved in relation to “G<sup>4</sup>”.
- The coupled system does tracking trajectories tests, in relation to the end effector regarding the “G<sup>4</sup>” coordinate.

The mentioned stages related to the subsystems and the homogenous transformations are shown in Fig. 2.

## 2.3 Position and Orientation Diagram

Figure 3 presents a general description of the position and orientation of the system, depicted by the relation of 4th transformation of global coordinates regarding to  $GA_{(4)} = \text{Trans} \left( x_G^{(4)}, y_G^{(4)}, z_G^{(4)} \right) GA_{(3)}$ .

## 2.4 Homogeneous Transformations Graph (HTG)

The third step of the methodology is the homogeneous transformation graph that in modular way allows

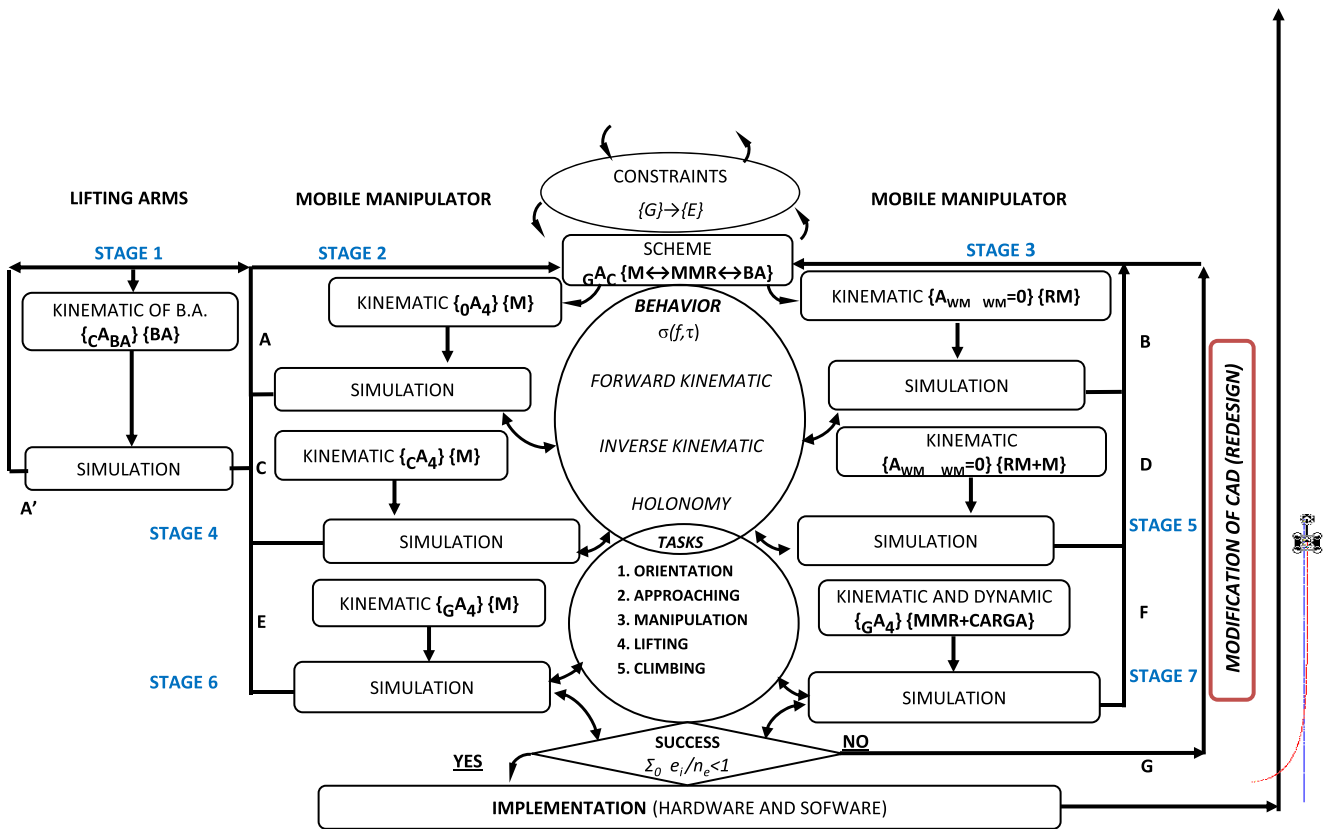


**Fig. 2** Master map of the MMR12-EOD robot. It is a diagram that shows the development of the mobile manipulator modeling and every subsystem is identified together with the

homogeneous transformation graph (HTG). Each stage is validated through simulation

to structure the subsystems that formed the mobile manipulator plus the added subsystem. This graph is an extension of transformation graph proposed to the manipulators kinematic by Robert Paul, in 1983 [25] and used in several works by Tadeusz Skodny [31]. The extension of Pauli’s graph allows getting the homogenous transformation graph for the kinematic modeling of wheeled mobile manipulators with any added subsystem. These transformations are

the central part of the methodology, because they give the relations with the “0” manipulator coordinates, “C” of mobile platform, the transformations of wheels and of lifting arms regarding to “C” and “C” regarding to “G<sup>4</sup>” as shown in Fig. 4. Afterwards are assignment coordinates systems to determine points that allow by mean of the suitable relations, obtain the coupled kinematic modeling of full system.

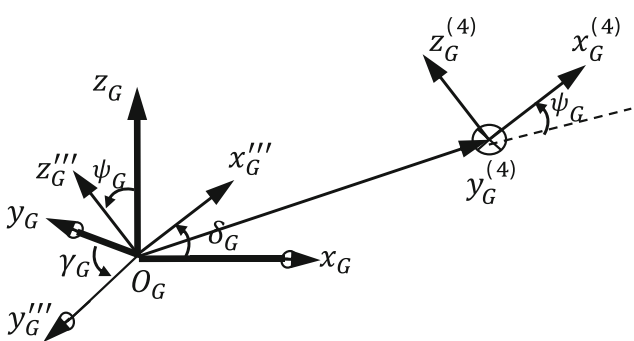


**Fig. 3** Description of the manipulator position movement in relation to global coordinates

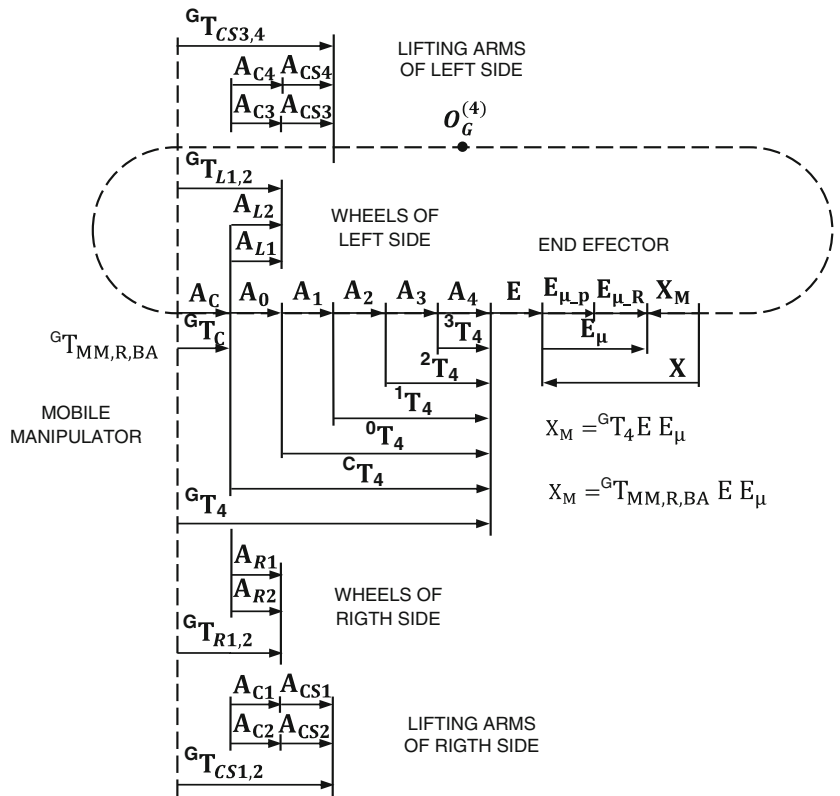
### 2.5 Kinematics Schemes of Operation Scenarios

In order to do the kinematic schemes of 5 real operation scenarios of the MMR12-EOD robot, it is necessary to consider its design parameters, shown in Table 1.

### 2.6 Kinematic Interactions

Table 2 shows the kinematic interaction parameters that are obtained by analyzing the subsystems coupling of the MMR12-EOD robot.

**Fig. 4** HTG for mobile manipulators. It allows structuring the subsystems that formed the mobile manipulator (*wheels and manipulator*) plus the added subsystem (*lifting arms*)



2.7 Forward and Inverse Kinematics

2.7.1 Forward Kinematics

Based on the homogenous transformation graph and the kinematic interactions table is the forward kinematic developed, being with the transformation  $A_C$ , which is the coordinate “C” and from these are depicted the transformations of the wheels, the lift arms and the manipulator, considering the end effector “E” with the load “ $E_\mu$ ”, as it is shown in Figs. 5 and 6.

a) *Mobile platform*

The homogenous transformation of the mobile platform is  $A_C = \begin{pmatrix} x_G^{(4)} & y_G^{(4)} & z_G^{(4)} \\ \rightarrow & x_C y_C z_C \end{pmatrix}$ , where  $A_C =$

**Table 1** Design parameters of mobile manipulator MMR12-EOD

| Configuration                   | Type                   | Degrees of freedom      |
|---------------------------------|------------------------|-------------------------|
| Mobile platform not articulated | Diferential locomotion | 4 (X, Y, Z, $\varphi$ ) |
| Manipulator                     | Articulated            | 4 (RPRR)                |
| Lifting arms                    | Articulated            | 4 (RR)                  |
| Total                           |                        | 12                      |

$\text{Trans}(x_{C0}, y_{C0}, z_{C0})\text{Rot}(z, \varphi)\text{Trans}(0, 0, \Delta\lambda_C)$  and its parameters are:  $x_{C0}$ (variable),  $y_{C0}$ (variable),  $z_C = \lambda_{C0} + \Delta\lambda_C$ ,  $z_{C0} = \lambda_{C0}(\text{const} > 0)$ ,  $\theta_{C1}$ (variable),  $l_{CS1}(\text{const.} > 0)$ ,  $\varphi$ (variable). The increment of  $\lambda_C$  depends on the following relation:

$$\Delta\lambda_C = \begin{cases} l_{CS1}S_{C1} - \lambda_{C0} + r & \text{for } l_{CS1}S_{C1} - \lambda_{C0} + r \geq 0, r_1 = r_2 = r_3 = r_4 = r = \text{constant} > 0 \\ 0 & \text{for other case} \end{cases} \quad (1)$$

Then, the transformation of the local coordinate is obtained,  $GT_C = A_C$  and so the transformations of the right and left wheels,  $GT_R = A_C A_R$  y  $GT_L = A_C A_L$ .

b) *Lifting arm in slopping surfaces*

The homogeneous transformation for lifting the arm is developed in relation to the local coordinate “C”. In Fig. 7, it is shown the lateral view of the mobile manipulator in the elevation position, were increment of  $\lambda_C$  is presented.

The parameters for the lifting arm of the right front side are as follows:  $A_{CS1} : \theta_{CS1}$ (variable),  $l_{CS1}(\text{const} > 0)$ , therefore the transformation of arm

**Table 2** Kinematics interactions of the MMR12-EOD robot. The parameters and their interaction as coupled system are used as basis of the forward and inverse kinematics

| Manipulator |                  |                  |                    | Interaction                       | Mobile platform and lifting arms |                |           |           |           |   |                       |
|-------------|------------------|------------------|--------------------|-----------------------------------|----------------------------------|----------------|-----------|-----------|-----------|---|-----------------------|
| Link        | $\alpha_i$ [rad] | $l_i$ [m]        | $\lambda_i$ [m]    | $\theta_i$ [rad]                  | $\varphi_i$ [rad]                | $\psi_i$ [rad] | $x_i$ [m] | $y_i$ [m] | $z_i$ [m] | $b_i$ [m]                                       | $d_i$ [m]             |
| C           | -                | -                | -                  | -                                 | $\varphi_c(\theta_R, \theta_L)$  | $\psi = -var$  | $x_c$     | $y_c$     | $z_c$     | $\lambda_c = 0.15,$<br>$\lambda_c(\theta_{cs})$ | -                     |
| $W_R$       | -                | -                | -                  | $\theta_{R1,2}$                   | -                                | -              | -         | -         | -         | $-b_{R1,2}$                                     | -                     |
| $W_L$       | -                | -                | -                  | $\theta_{L1,2}$                   | -                                | -              | -         | -         | -         | $b_{L1,2}$                                      | -                     |
| $C_1$       | $-\pi/2$         | $l_{cs} = 0.33$  | 0                  | $\theta_{C1,2,3,4}$               | -                                | -              | -         | -         | -         | -   | -                     |
| $CS_1$      | 0                | $l_{csi} = 0.44$ | 0                  | $\theta_{C_{s1,2,3,4}}$           | -                                | -              | -         | -         | -         | -   | $d_{R1,2} \ d_{L1,2}$ |
| 0           | $\pi/2$          | $-l_0 = -0.33$   | $\lambda_0 = 0.16$ | 0                                 | -                                | -              | -         | -         | -         | -   | -                     |
| 1           | $\pi/2$          | 0                | 0                  | $\theta_1 = \theta'_1 + 90^\circ$ | -                                | -              | -         | -         | -         | -   | -                     |
| 2           | $-\pi/2$         | 0                | $\lambda_2 = 0.4$  | 0                                 | -                                | -              | -         | -         | -         | -   | -                     |
| 3           | $\pi/2$          | $l_3 = 0.15$     | 0                  | $\theta_3 = -var$                 | -                                | -              | -         | -         | -         | -   | -                     |
| 4           | 0                | 0                | 0                  | $\theta_4$                        | -                                | -              | -         | -         | -         | -   | -                     |
| E           | 0                | 0                | $\lambda_5 = 0.38$ | 0                                 | -                                | -              | -         | -         | -         | -   | -                     |
| $E_{\mu P}$ | 0                | 0                | $\lambda_6 = 0.05$ | 0                                 | -                                | -              | -         | -         | -         | -   | -                     |
| $E_{\mu R}$ | $\pi/2$          | 0                | 0                  | $\theta_\mu$                      | -                                | -              | -         | -         | -         | -   | -                     |

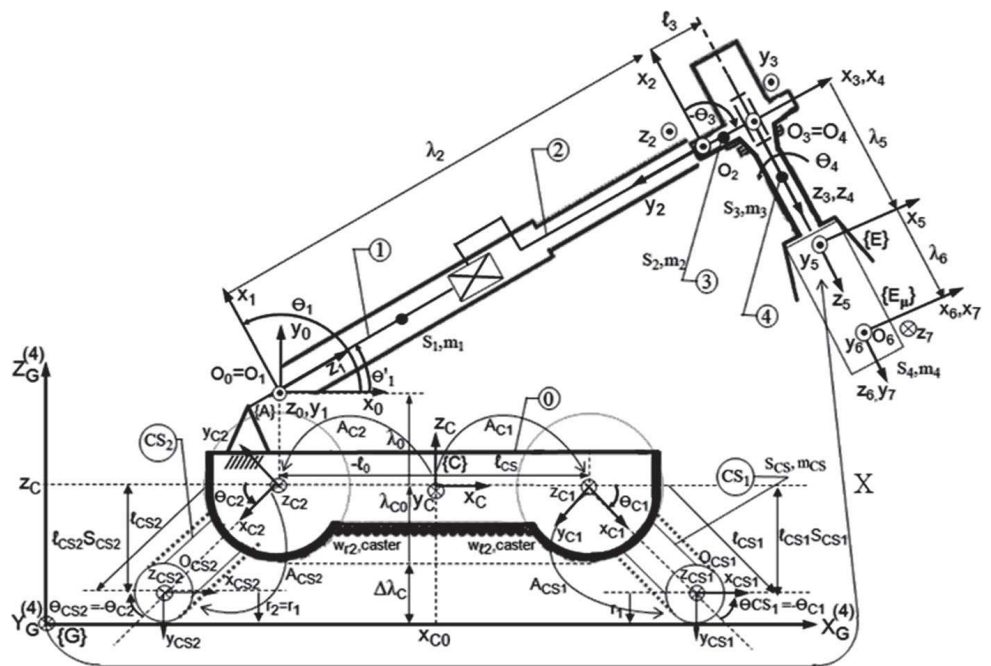
1 in relation to the global coordinate is  $GT_{CS1} = A_C A_{C1} A_{CS1}$ . Similarly are the relations for the second, third and fourth lifting arm carried out.

c) Manipulator

It is presented the respective transformations of the 4 degree of freedom regarding to coordinate "0",

in relation to the "C" coordinate. The homogenous transformation from "C" to "0",  $A_0 = (x_c y_c z_c \rightarrow x_0 y_0 z_0)$ , depends on the following parameters:  $\theta_0 = 0^\circ$ ,  $\lambda_0 = \text{const} > 0$ ,  $l_0 = \text{const} < 0$ ,  $\alpha_0 = 90^\circ$ ,  $A_1 = (x_0 y_0 z_0 \rightarrow x_1 y_1 z_1)$ , depends on the following parameters:  $\theta_1$  (variable),  $\lambda_1 = 0$ ,  $l_1 = 0$ ,  $\alpha_1 = 90^\circ$ , the transformation  $A_2 = (x_1 y_1 z_1 \rightarrow x_2 y_2 z_2)$ , depends on

**Fig. 5** Lateral view of the MMR12-EOD robot in lifting position



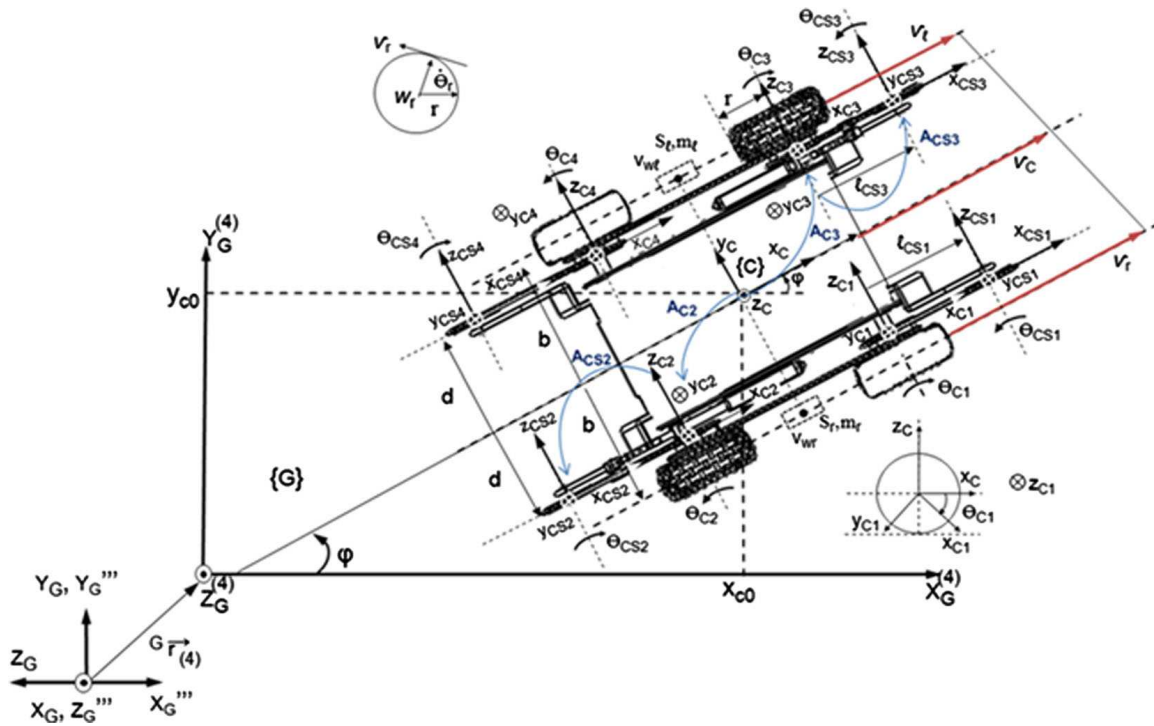


Fig. 6 MMR12-EOD robot in top view

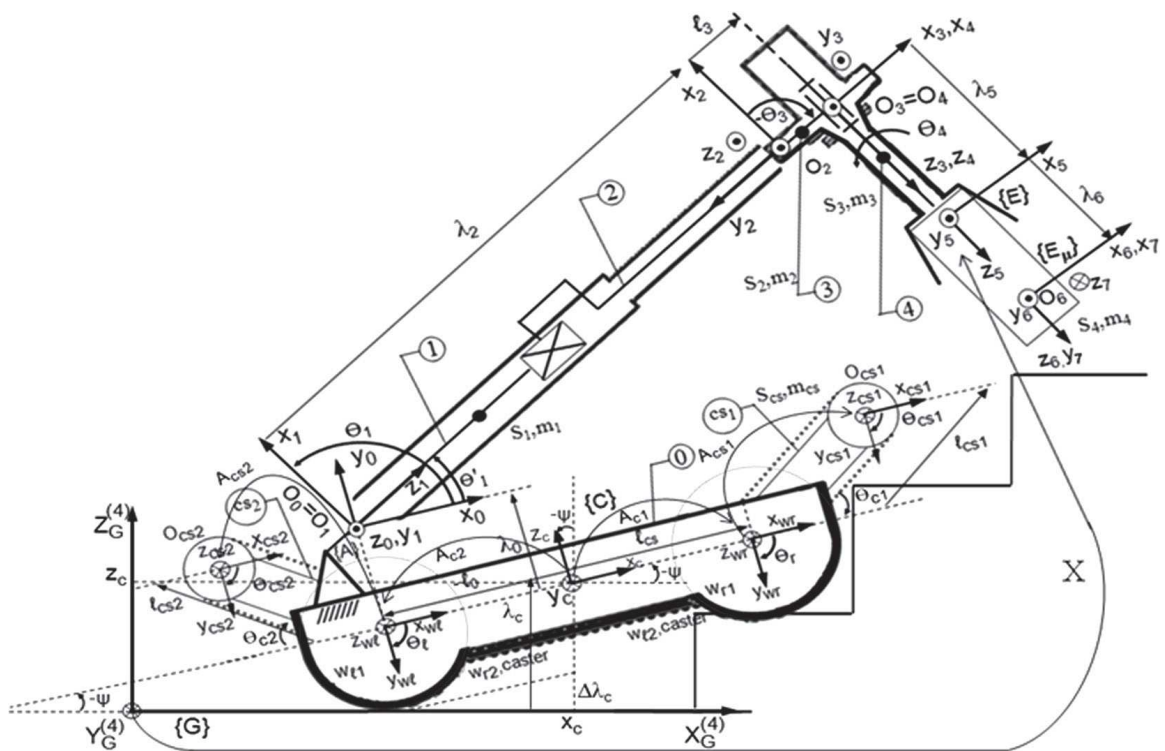


Fig. 7 Lateral view, driving the MMR12-EOD robot in climbing operation



the following parameters:  $\theta_2 = 0^\circ$ ,  $\lambda_2$ (variable),  $l_2 = 0\alpha_2 = -90^\circ$ , the  $A_3 = (x_2y_2z_2 \rightarrow x_3y_3z_3)$  transformation depends on the following parameters:  $\theta_3$ (variable),  $\lambda_3 = 0$ ,  $l_3$ (const  $> 0$ ),  $\alpha_3 = 90^\circ$  and the transformation  $A_4 = (x_3y_3z_3 \rightarrow x_4y_4z_4)$  depends on the following parameters:  $\theta_4$ (variable),  $\lambda_4 = 0$ ,  $l_4 = 0\alpha_4 = 0^\circ$ .

The transformations of end effector in relation to the 4 degree of freedom of manipulator are given by:  $E = (x_4y_4z_4 \rightarrow x_5y_5z_5)$ , where,  $E = \text{Trans}(0,0,\lambda_5)$  and its parameters:  $E : \theta_5 = 0^\circ$ ,  $\lambda_5 = \text{const} > 0$ ,  $l_5 = 0\alpha_5 = 0^\circ$ . In order to obtain the homogeneous transformation that relates the load to the end effector the next equation is used:  $E_\mu = E_{\mu P}E_{\mu R}$ , where  $E_\mu$  is the total load, constituted by  $E_{\mu P}$  y  $E_{\mu R}$ , which are

the load deployed as prismatic joint and rotational, respectively. The parameters of prismatic joint are the following:  $E_{\mu P}$ :  $\theta_6 = 0^\circ$ ,  $\lambda_6 = \text{const} > 0$ ,  $l_6 = 0\alpha_6 = 0^\circ$ , and the parameter of rotational joint is:  $E_{\mu R}$ :  $\theta_7 = 0^\circ$ ,  $\lambda_7 = 0$ ,  $l_7 = 0\alpha_7 = 90^\circ$ .

The transformation of the manipulator is  $T_4$ , using the trigonometric simplification  $\text{Cos}(A + B) = C_A C_B - S_A S_B = C_{AB}$ ,  $\text{Sin}(A + B) = C_A S_B + S_A C_B = S_{AB}$  is the transformation obtained from manipulator to global coordinates given by  $GT_4 = A_C C T_4$ . The transformation of the end effector with the load is determined by  $E_\mu = E_{\mu P}E_{\mu R}$ . Finally, the homogenous transformation from load "X" in the end effector regarding to global coordinates is obtained and presented in Eq. 2.

$$X_M = GT_4 E E_\mu$$

$$= \begin{bmatrix} S_4 S_C + C_C C_{13} C_4 & C_C S_{13} & C_C C_{13} S_4 - C_4 S_C & x_C + C_C(S_1 \lambda_2 + l_3 C_{13} - l_0) + C_C \lambda_5 S_{13} + C_C \lambda_6 S_{13} \\ S_C C_{13} C_4 - C_C S_4 & S_C C_{13} & S_C C_{13} S_4 + C_4 C_C & y_C + S_C(S_1 \lambda_2 + l_3 C_{13} - l_0) + S_C \lambda_5 S_{13} + S_C \lambda_6 S_{13} \\ S_{13} C_4 & -C_{13} & S_{13} S_4 & z_{C0} + \Delta \lambda_C + \lambda_0 - \lambda_5 C_{13} - C_1 \lambda_2 + l_3 S_{13} - \lambda_6 C_{13} \\ 0 & 0 & 0 & 1 \end{bmatrix} \tag{2}$$

### 2.7.2 Inverse Kinematics

The inverse kinematics scheme is shown in Fig. 8. From this scheme, the equations that relate the Cartesian coordinates form task space regarding to joint parameters are obtained and listed from Eqs. 3–11. The equations show how the mobile manipulator estimates the coordinates of end effector to the Cartesian coordinates. The inverse kinematic was developed using the homogenous transformations.

$$\varphi = \tan^{-1} \left( \frac{dy}{dx} \right) \tag{3}$$

$$\theta_3 = \cos^{-1} \left[ \frac{dx^2 + dy^2 + dz^2 - \lambda_2^2 - \lambda_5^2}{-2\lambda_2 \lambda_5} \right] \tag{4}$$

$$\lambda_2 = \frac{dz + \lambda_0 - \lambda_5 C_3 + l_3 S_3}{C_3} \tag{5}$$

$$E = \tan^{-1} \left( \frac{l_3}{\lambda_5} \right); K = 180 - 90 - E1; h = \left( \frac{l_3}{S_E} \right); \tag{6}$$

$$P = 180 - K - q_3; r = \sqrt{h^2 + d_2^2 - [2hd_2 C_{P1}]}; \tag{7}$$

$$d = \cos^{-1} \left( \frac{h^2 + r^2 - d_2^2}{2hr} \right); q'_1 = 180 - P - d_1; \tag{8}$$

$$q''_1 = \sin^{-1} \left( \frac{d_z + d_0 - d_C}{r} \right); q_1 = q'_1 + q''_1 \tag{9}$$

$$x_C = d_X - C_C(\lambda_2 S_1 - l_0 + l_3 C_{13} + \lambda_5 S_{13}) \tag{10}$$

$$y_C = d_Y - S_C(\lambda_2 S_1 - l_0 + l_3 C_{13} + \lambda_5 S_{13}) \tag{11}$$

Last equations were obtained by means of the graphical scheme presented in Fig. 8, where Eq. 7 represents the variables P and r in degrees that were assigned to help to obtain the angles to the deduction of the inverse kinematics.

### 2.8 Constraints

The differential kinematics in relation to  $Z_G^{(4)}$  can be calculated based on nonholonomic constraints. Those

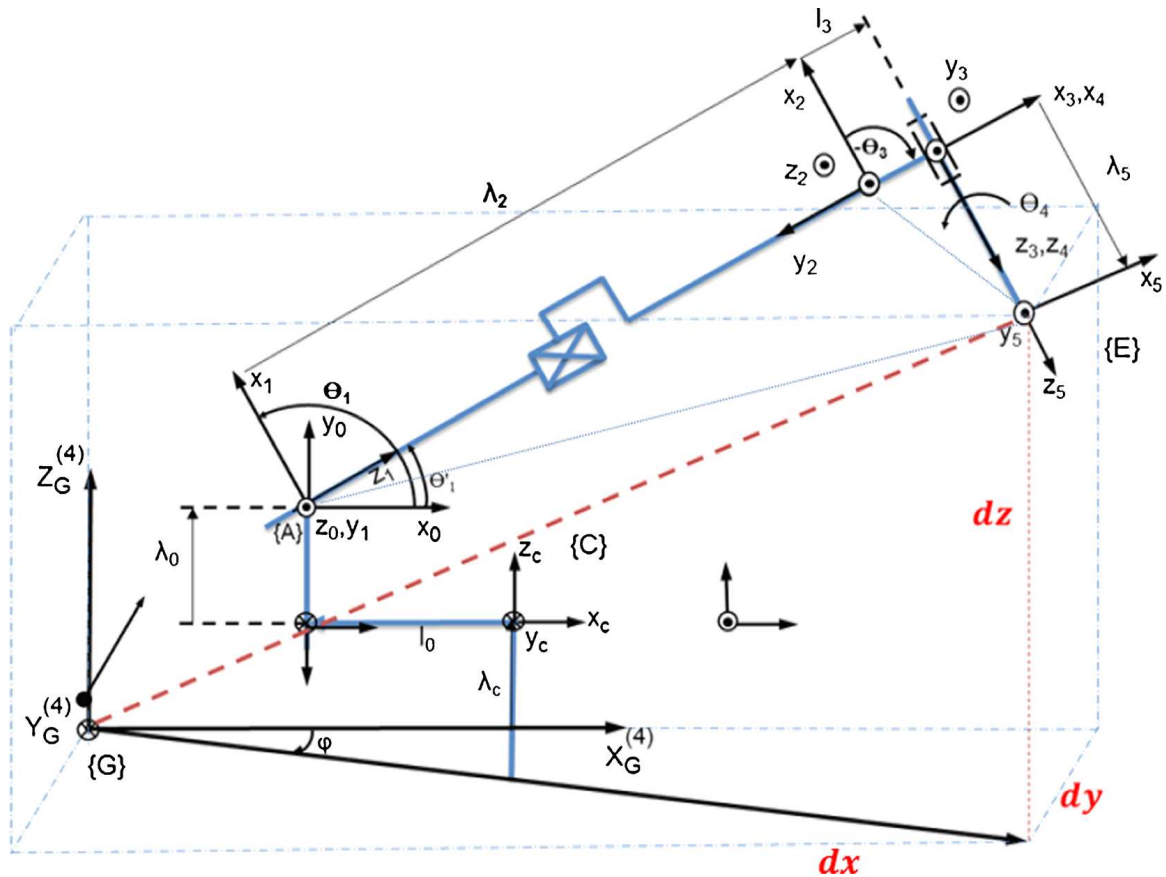


**Fig. 8** The inverse kinematic scheme was developed using homogeneous transformations and the derived equations of the forward kinematics

do not have integral solution and represent more degrees than the controllable degrees of freedom [7, 25]. In order to relate the velocities from the system,

it is considered that the orientation angles regarding to global coordinates are;  $(x_G, \delta_G)$   $(y_G, \varphi_G)$   $(z_G, \gamma_G)$ , assuming that the position and orientation or local

**Table 3** Constraints equations of the MMR12-EOD robot

|   |   |
|---|---|
| <p>One constraint is that the mobile platform must move in the direction of the axis of symmetry of itself without sliding of any the wheels in relation to ground, where <math>(x_{C0}, y_{C0}, z_{C0})</math> are the coordinates of the center of mass of mobile platform, <math>\varphi</math> is the heading angle of the platform measured from the <math>X_G^{(4)}</math> axis of the local coordinates.</p> | $\dot{y}_{C0} \cos \varphi - \dot{x}_{C0} \sin \varphi = 0 \tag{12}$  |
| <p>The other two are the rolling constraints, i.e., the driving wheels do not slip, where <math>\theta_r, \theta_l</math> are the angular displacement of the right and left wheels, respectively.</p>  | $\dot{x}_{C0} \cos \varphi + \dot{y}_{C0} \sin \varphi + \dot{\varphi} b = \dot{\theta}_r r \tag{13}$ $\dot{\varphi} = \frac{r}{2b} (\dot{\theta}_r - \dot{\theta}_l) \tag{14}$ |

reference in relation to the global reference are constant in the robot movement, and  $\dot{\theta}_{C1} = 0, \dot{\theta}_{CS1} = 0$ . Table 3 shows the constraints equations [25]:

Next, the Eq. 15 shows the twelve variables for the Jacobian (16).

$$q = [x_{C0} \ y_{C0} \ \varphi_C \ \theta_r \ \theta_1 \ z_{C0} \ \theta_{C1} \ \theta_{CS1} \ \theta_1 \ d_2 \ \theta_3 \ \theta_4]^T, \tag{15}$$

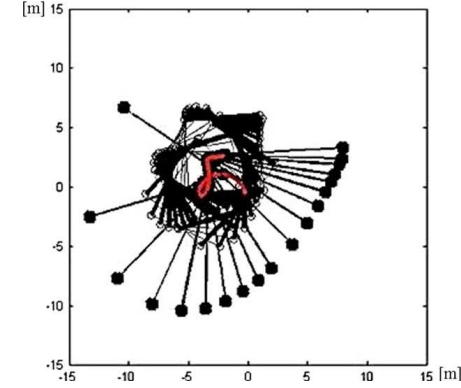
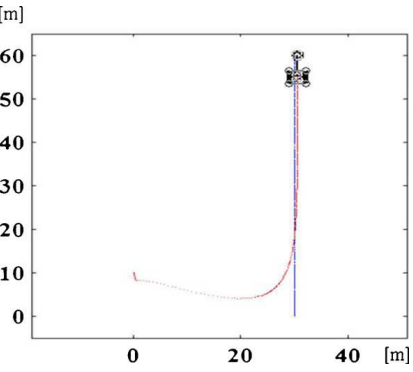
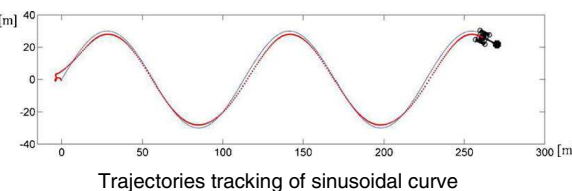
$$J = \begin{bmatrix} -\sin \varphi & \cos \varphi & 0 & 0 & 0 & 0 & 0 & 0 & 0 & 0 & 0 & 0 \\ -\cos \varphi & -\sin \varphi & -b & r & 0 & 0 & 0 & 0 & 0 & 0 & 0 & 0 \\ 0 & 0 & -1 & \frac{r}{2b} & -\frac{r}{2b} & 0 & 0 & 0 & 0 & 0 & 0 & 0 \end{bmatrix} \tag{16}$$

It is known that  $J(q)\dot{q} = 0$  and as  $J(q)$  is a square matrix, then:  $J_1^{-1} = \frac{1}{|J_1|}[\text{adj}(J_1)]^T, [\text{adj}(J_1)]^T$ , because of the determinant of  $J_1$  results  $|J_1| = -1$ , then the mobile manipulator has good manipulability according to the mobile platform [13].  $J(q) = [J_1(q), J_2(q)]$ . Finally we have  $J_{12}(q) = -J_1^{-1}(q)J_2(q)$ .

### 2.9 Dynamic Parameters

The dynamic model was done using Lagrange's computational algorithm, based on the homogenous transformations and the interactions table, which is presented in this work in 10 steps. We will use the letter

**Table 4** Tasks of orientation and tracking trajectories

|   |  |
|---|--|
|  <p>A 2D plot showing multiple black trajectories spiraling inward towards a central point. The axes range from -15 to 15 meters. A red line indicates the reference path.</p>  | <p>Sample time of: <math>t_m = 200</math> s. The reference C, is located in:<br/> <math>y_{desired} = 0</math><br/> <math>x_{desired} = 0</math><br/>                     Mean error of 40 mm.</p>                     |
| <p>Trajectories tracking about its center</p>   |  |
|  <p>A 2D plot showing a single trajectory starting at (0,0) and moving along a path that curves upwards to a point at approximately (30, 60). The x-axis ranges from 0 to 40 meters, and the y-axis from 0 to 60 meters.</p> | <p><math>t_m = 200</math> s. The reference, is located in:<br/> <math>y_{desired} = t</math><br/> <math>x_{desired} = 30</math><br/>                     Mean error of 2.0 mm.</p>                                     |
| <p>Following a straight trajectory</p>  |  |
|  <p>A 2D plot showing multiple black trajectories following a sinusoidal wave pattern. The x-axis ranges from 0 to 300 meters, and the y-axis from -40 to 40 meters. A red line indicates the reference path.</p>            | <p><math>t_m = 200</math> s. The reference, is located in:<br/> <math>y_{desired} = 30 \sin(0.25 t)</math><br/> <math>x_{desired} = 40 \cos(0.25 t) + 2.5 t</math><br/>                     Mean error of 2.37 mm.</p> |
| <p>Trajectories tracking of sinusoidal curve</p>  |  |

L to describe each step. L1 is the description of each link of the interaction table HTG. L2 is the classification of the homogeneous transformation. L3 is the determination of the primary matrices of  $U_{ij}$ . L4 is the determination of the secondary matrices  $U_{ijk}$ . L5 describes the pseudo inertial matrices of each link. L6 is the inertia matrix  $M(q) = [d_{ij}]$ . L7 is the determina-

tion of the Coriolis and centrifuge forces parameters  $h_{ikm}$ . L8, is the determination the Coriolis and centrifuge forces. L9 is the determination of the gravity matrix  $G(q) = [c_i]^T$  and L10 is the dynamic equation  $V(q, \dot{q}) = [h_i]^T$ .

$$M(q)\ddot{q} + V(q, \dot{q})\dot{q} + G(q) = E(q)\tau - A^T(q)\lambda \quad (17)$$

$$\begin{bmatrix} d_{11} & \dots & d_{112} \\ \vdots & \dots & \vdots \\ d_{121} & \dots & d_{1212} \end{bmatrix} \ddot{q} + \begin{bmatrix} h_1 \\ \vdots \\ h_{12} \end{bmatrix} \dot{q} + \begin{bmatrix} c_1 \\ \vdots \\ c_{12} \end{bmatrix} = \begin{bmatrix} 0 & 0 \\ \vdots & \vdots \\ 1 & 0 \\ 0 & 1 \\ \vdots & \vdots \\ 0 & 0 \end{bmatrix} \begin{bmatrix} \tau_x \\ \vdots \\ \tau_4 \end{bmatrix} - \begin{bmatrix} -S_C & C_C & 0 & 0 & 0 & \dots & 0 \\ -C_C & -S_C & -b & r & 0 & \dots & 0 \\ 0 & 0 & b & 0 & r & \dots & 0 \end{bmatrix} \quad (18)$$

The dynamic equation is described in Eq. 17. Equation 18 shows a more detailed form of the corresponding matrices.

$$\ddot{q} = M(q)^{-1}[E(q)\tau - A^T(q)\lambda - V(q, \dot{q})\dot{q} - G(q)] \quad (19)$$

$$S(q) = \begin{bmatrix} -S_C & C_C & 0 & 0 & 0 & \dots & 0 \\ -C_C & -S_C & -b & r & 0 & \dots & 0 \\ 0 & 0 & b & 0 & r & \dots & 0 \end{bmatrix}. \quad (20)$$

### 2.10 Consolidation of Dynamic Equation

The two columns  $S(q)$  are the null space of  $A(q)$  and are linear independent.  $q$  could be expressed as a lineal combination of two columns of  $S(q)$ .

$$\dot{q} = S(q)v$$

After derivation, it turns out in:

$$\ddot{q} = S(q)\dot{v}(t) + \dot{S}(q)v(t)$$

Substituting it in Eq. 14 gives way to Eqs. 18 and 19:

$$\begin{aligned} & S^T(q) \\ & (M(q)S(q)\dot{v}(t) + M(q)\dot{S}(q)v(t) + V(q, \dot{q})\dot{q} + G(q)) \\ & = (E(q)\tau - A^T(q)\lambda)S^T(q) \end{aligned} \quad (21)$$

$$\begin{aligned} & S^T(q) (M(q)S(q)\dot{v}(t) + M(q)\dot{S}(q)v(t) + V(q, \dot{q})\dot{q} \\ & + G(q)) = \tau \end{aligned} \quad (22)$$

In order to validate (22), it was verified that the corresponding inertia matrix  $M(q)$  satisfy the next properties: 1) it is square, 2) it symmetrical  $M^T(q) = M(q)$ , 3) it is not singular due to the fact that the determinant of the inertia matrix is positive and equal to the determinant of its transpose matrix  $det(M(q)) = 8.0644e + 021 > 0 = det(M(q)^T) = 8.0644e + 021 > 0$ , 4) it is positive defined  $d_{11}(q) > 0$ .

### 2.11 Real Experimentation and Positioning Simulation

The real experimentation and simulation of the mobile manipulator positioning is done according to five real operation tasks. In order to do these activities the control strategy published by Yamamoto was used [7], where the control and coordination of movement from mobile manipulators was presented in 2004. Using the vector in the state space  $x = [q^T \ v^T]^T$ , we can represent the constraints and movement equations from mobile manipulator in the state space:

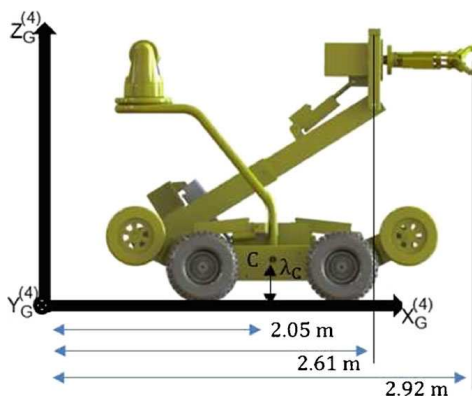
$$\dot{x} = \begin{bmatrix} Sv \\ f_2 \end{bmatrix} + \begin{bmatrix} 0 \\ (S^TMS)^{-1} \end{bmatrix} \tau \quad (23)$$

where  $f_2 = (S^TMS)^{-1}(-S^TMSv - S^TV)$ . This equation is then simplified as:

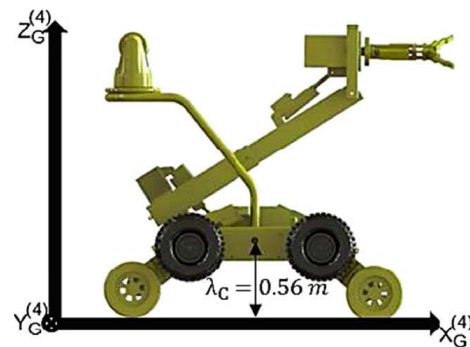
$$\dot{x} = \begin{bmatrix} Sv \\ 0 \end{bmatrix} + \begin{bmatrix} 0 \\ I \end{bmatrix} u \quad (24)$$

Last equation is used to apply the feedback  $\tau = S^TMS(u - f_2)$ . According to Eq. 24 a new input  $u$  is

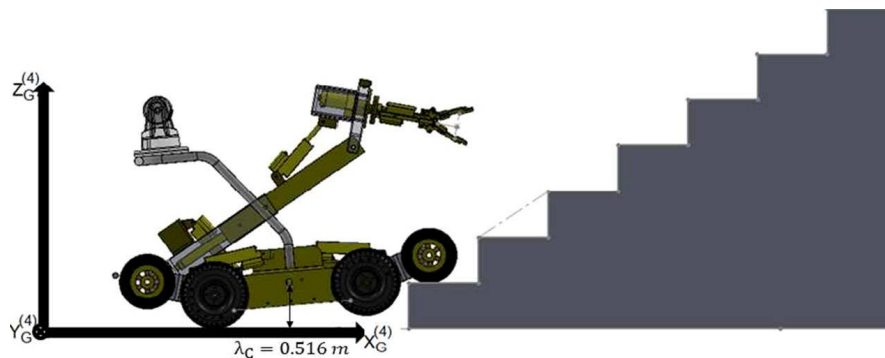
**Table 5** Manipulation, lifting and climbing



Mean error of 0.050 mm in the manipulation task.



Mean error of 0.020 mm in the lifting task.



Mean error of 40 mm in the climbing task.

assumed, which linearizes (23). In this way we can use the desired trajectory  $y^d$  in order to feedback the error  $e = y^d - y$ .

$$\ddot{y} = v = \ddot{y}^d + K_d(\dot{y}^d - \dot{y}) + K_p(y^d - y) \quad (25)$$

From Eq. 21,  $v$ ,  $u$  and then  $\dot{x}$  can be calculated. By integrating  $\dot{x}$  then  $x$  is obtained.

a) Orientation (stage 2, task 1). The actuated wheels have differential steering, so that  $v_r = -v_l$ . It allows that the mobile platform rotates around its  $z$  coordinate, in an ideal diameter of  $\phi = 1,130$  mm. It is assumed that the mobile manipulator movement is carried out horizontally and the wheel is in contact with the floor in only one point. Wheels deformation is not considered, meaning that the contact point with the floor is  $v = 0$ , there is no slippage, and the direction axis is orthogonal the surface. The wheels are connected by a rigid body (chassis).

b) Approaching / Trajectory tracking (stage 4, task 2). The system executes the tracking the desired trajectory, based on the transformation  $GT_C =$

**Table 6** Real experimentation of manipulation, lifting and climbing tasks

| 30 samples   | Deviations |            |
|--|------------|------------|
| 1. In the test of orientation were measures errors of: | Error min. | Error max. |
|  | 40 mm      | 80 mm.     |
| 2. Approaching (trajectories tracking).                | Error min. | Error max. |
|  | 0.5 mm     | 8 mm.      |
| 3. Manipulation (positioning).                         | Error min. | Error max. |
|  | 0.5 mm     | 8 mm.      |
| 4. Lifting.  | Error min. | Error max. |
|  | 4 mm       | 6 mm.      |
| 5. Climbing.   | Error min. | Error max. |
|  | 4.6 mm     | 8 mm.      |

$A_C$ , the mobile platform is moved according this equation:  $q_{MR} = [xyz\varphi_C\theta_r\theta_1]^T$ .

- c) Manipulation (stage 4, task 3). In the rank:  $x = 2.5, y = 2.5, z = 1.5$  m, the kinematic is given by:  $X_M = GT_4E E_\mu$  by main the equation:  $q_M = [\varphi_C\theta_1d_2\theta_3\theta_4]^T$ .
- d) Lifting the mobile manipulator in the Rank from 0.15 up to 0.52 m. based in the transformation  $GT_C = A_C$ ,  $z$  is given by  $z_C = \lambda_{C0} + \Delta\lambda_C$  (which is variable),  $z_{C0} = \lambda_{C0} = \text{const} > 0, \theta_{C1}(\text{variable}), I_{CS1} = \text{const} > 0, \varphi(\text{variable})$ , where the increment  $\Delta\lambda_C$  of  $z$ , depends of lifting arms.
- e) In the lifting test, the frontal arms raise the mobile manipulator from  $\lambda_C = 0.15$  m to  $\lambda_C = 0.47$  m. The mobile manipulator with mass  $m$  is moved on the slope with an angle  $\psi$  (to the horizontal) given by the transformation  $CT_{CS1}$ , and the equation  $F_{climb} = mg(\sin\psi + \mu\cos\psi)$ , where  $g$  is the gravity, when  $\theta_{CS} > 60^\circ, \lambda_C + (\Delta_C = I_{CS1} + \sin\theta_{CS})$

### 3 Results

The reference values for every task were taken from the forward kinematics. The parameters for the local “C” coordinate, which is the base to obtain the reference values are the following:  $A_C : x_{C0} = 2, y_{C0} = 2, z_C = \lambda_{C0} + \Delta\lambda_C, z_{C0} = \lambda_{C0} = 0.15, \theta_{C1} = \frac{\pi}{2}, I_{CS1} = 0.44, \varphi = \frac{\pi}{4}, \varphi = 20\pi$ .

$$\Delta\lambda_C = \begin{cases} I_{CS1}S_{C1} - \lambda_{C0} + r & \text{for } I_{CS1}S_{C1} - \lambda_{C0} + r \geq 0, r_1 = r_2 = r_3 = r_4 = r = 0.08 \\ 0 & \text{other case} \end{cases} \tag{26}$$

- a) Equation 27 shows how the platform mobile rotates about its axis:

$$GT_C = A_C = \begin{bmatrix} 1 & 2.4493e - 015 & 0 & 0 \\ -2.4493e - 015 & 1 & 0 & 0 \\ 0 & 0 & 1 & 0.15 \\ 0 & 0 & 0 & 1 \end{bmatrix} \tag{27}$$

**Table 7** Simulation and real experimentation

| Task                                   | Performance                                       |   | Comments   |
|--|---|---|--|
|  | Simulation ( $\bar{e}$ and RMS)                   | Real system ( $\bar{e}$ and RMS)                  |  |
| 1. Orientation.                        | 40 mm and 40.16 mm                                | 60 mm and 60.09 mm                                | Error due to wheel slip on the floor.  |
| 2. Approaching.                        | 2.37 mm and 2.38 mm                               | 6.5 mm and 6.52 mm                                | Two tests were performed at 0.5 m/s.   |
| 3. Manipulation.                       | 0.050 mm and 0.050 mm                             | 4.25 mm and 4.25 mm                               | The large error is due to slipping of wheels on the floor.   |
| 4. Lifting.                            | 0.02 mm and 0.02 mm                               | 5 mm and 5.04 mm                                  | Due to adjustment and the weight from mobile manipulator.  |
| 5. Climbing.                           | 0.04 mm and 0.041 mm                              | 6.3 mm and 6.31 mm                                | It is due to deformation of the rear wheels and its adjustment, and to the weight of the mobile manipulator. |
| Dynamic analysis with the CAE software | 8.5 mm 8.53 mm<br>With load                       | 16.41 mm 16.45 mm<br>Without load                 | The greatest variation occurs in Z.  |
|  | The center of mass varies in a diameter of 60 mm. | The center of mass varies in a diameter of 40 mm. | It was validated to the fullest extent and in the normal state of the prismatic joint.                       |
|  | The stress due to load is 14 Kpa.                 | The stress due to load is 7 kpa.                  |  |
|  | The $\lambda_2$ deformation is of 1.055 mm.       | The $\lambda_2$ deformation is of 0.03 mm.        |  |

According to the manual B.L.A.D.E. of Secretariat of National Defense (Mexico) the artifact manipulation error it is considered around 10 mm

- b) Equation 28 is the transformation of the platform according to the parameters:  $x_C = 2, y_C = 2, \lambda_{C0} = 0.15, \varphi_C = \frac{\pi}{4}, \theta_R = 2\pi, \theta_L = -2\pi, b = 0.4, \Delta\lambda_C = 0$

$$GT_C = A_C = \begin{bmatrix} 0.7071 & -0.7071 & 0 & 2 \\ 0.7071 & 0.7071 & 0 & 2 \\ 0 & 0 & 1 & 0.15 \\ 0 & 0 & 0 & 1 \end{bmatrix} \quad (28)$$

- c) Equation 29 is the transformation of the Manipulator with end effector:  $x_C = 2, y_C = 2, \lambda_{C0} = 0.15, \varphi_C = \frac{\pi}{4}, \lambda_0 = 0.16, l_0 = 0.33, \theta_1 = \frac{3\pi}{4}, \lambda_2 = 1.4, \theta_3 = -\frac{\pi}{2}, l_3 = 0.15, \theta_4 = \frac{\pi}{2}, \theta_{C1} = \frac{\pi}{2}, l_{CS1} = 0.44, r = 0.08, \lambda_5 = 0.38, \lambda_6 = 0.25,$

$$X_M = GT_4 EE_\mu = \begin{bmatrix} 0.7071 & 0.5000 & 0.5000 & 2.8567 \\ -0.7071 & 0.5000 & 0.5000 & 2.8567 \\ 0 & -0.7071 & -0.7071 & 1.3305 \\ 0 & 0 & 0 & 1 \end{bmatrix} \quad (29)$$

- d) Equation 30 is the transformation when the platform is lifting:  $x_C = 0, y_C = 0, \theta_{C1} = \frac{\pi}{2},$

$$GT_C = A_C = \begin{bmatrix} 0.7071 & -0.7071 & 0 & 0 \\ 0.7071 & 0.7071 & 0 & 0 \\ 0 & 0 & 1 & 0.5200 \\ 0 & 0 & 0 & 1 \end{bmatrix} \quad (30)$$

- e) Equation 31 is the transformation for climbing:  $x_C = 0, y_C = 0, \lambda_{C0} = 0.15, \varphi_C = \frac{\pi}{4}, \theta_{C1} = \frac{\pi}{2}, \theta_{CS1} = -\frac{\pi}{2}, d = 0.35, l_{CS} = 0.33, l_{CS1} = 0.44, r = 0.10$

$$GT_{CS1} = \begin{bmatrix} 0.7071 & 0 & -0.7071 & 0 \\ 0.7071 & 0 & 0.7071 & 0 \\ 0 & -1 & 0 & 0.47 \\ 0 & 0 & 0 & 1 \end{bmatrix} \quad (31)$$

Subsequently, the behavior of the mobile manipulator is simulated using (22), from which the respective errors of each area are obtained (Tables 4, 5 and 6).

In Table 7 the results of real experimentation in the mobile manipulator are shown, focused in the maximum and minimum errors according to the reference values.

In Fig. 9, it is shown the positioning test of the mobile manipulator, whereas a target was positioned

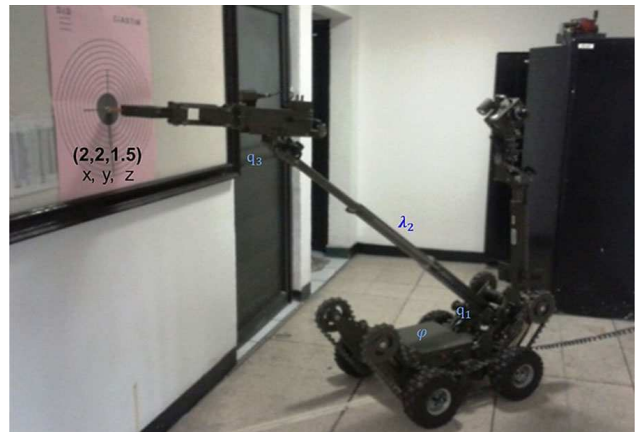


Fig. 9 Mobile manipulator in real experimentation. A set of 30 samples were carried out in order to validate simulation

at the wall localized in coordinates ( $x = 2, y = 2$  and  $z = 1.5$ ). In the initial setup, the robot was placed with an angle of  $45^\circ$  regarding to the wall (global coordinates) using stages 3 and 4 of the master map. The final coordinates of the end effector were established from the beginning of the experimentation.

### 4 Discussion

The real experimentation was done on the floor surface, which helped in the measurement of the register parameters. In Table 8, it is presented the comparison of errors of the simulations and real experimentation of 5 tasks. For each task, 30 tests were carried out,

Table 8 Summary of simulation and real experimentation errors

| Comparison of simulation and real experimentation |            |          |
|---|------------|----------|
| Tasks   | Difference |          |
| 1. Orientation.                                   | $\bar{e}$  | 20 mm    |
|   | RMS        | 19.95 mm |
| 2. Approaching.                                   | $\bar{e}$  | 4.13 mm  |
|   | RMS        | 4.15 mm  |
| 3. Handling.                                      | $\bar{e}$  | 4.2 mm   |
|   | RMS        | 4.2 mm   |
| 4. Lifting.                                       | $\bar{e}$  | 4.98 mm  |
|   | RMS        | 5.02 mm  |
| 5. Climbing.                                      | $\bar{e}$  | 6.26 mm  |
|   | RMS        | 6.28 mm  |

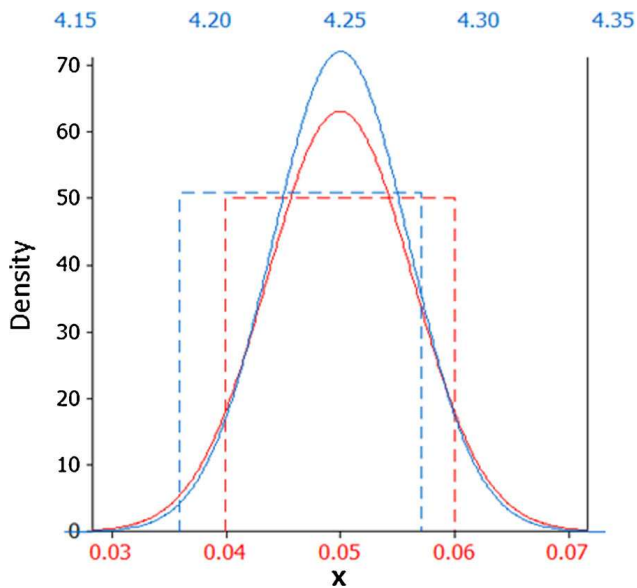


**Fig. 10** Simulation and real experimentation in the manipulation task. The blue continuous line represents the normal distribution and blue dotted line represents the uniform distribution, both in the real experimentation. The red continuous line represents the normal distribution and red dotted line represents the uniform distribution, both in the real simulation

(according to these tests the kinematic modeling of the robot is validated).

In Table 8, it is shown the difference of errors from simulated and real experimentation from the 5 assessed tasks. Figure 10 shows the simulation results in blue color and the experimentation in red color including the media and R.M.S. errors.

## 5 Conclusions

A methodology for positioning the multiarticulated mobile manipulator by means of the kinematic model is defined, explained and assessed, where the use of a novel scheme to devise the homogenous transformations provides a structure for the forward kinematics. The methodology has the following advantages: (1) gives a big picture of the mechatronic design when the modeling and simulation of a mobile manipulator is developed; (2) simplifies the obtained homogenous transformation when it is required; (3) allows to determine the interaction parameters when it is necessary to consider the coupled schemes; (4) ease the kinematic modeling when any added subsystem is incorporated, in the analysis of performance index based in the error of the real operation scenarios:

The simulations has an error of 3.47 mm regarding to the references values, while the real experimentation has an error of 7.91 mm, it is an permissible error in relation with the 10 mm that is specified in the deactivation tasks [32, 33]. The maxim deformation of the manipulator with load of 10 kg was 1 mm.

The main contribution of this work is the development of the coupled kinematic model for a wheeled mobile manipulator of  $12^\circ$  of freedom, also the extension of the homogeneous transformation graph that makes modular the establishing of transformation for the kinematics of mobile manipulators, and finally to propose a methodology capable to model the positioning of the mobile manipulators in real operation scenarios.

The total increment  $Z_c$  (in local coordinates) respect to the global coordinates is function of  $\lambda c_0$  (wheels radio) and  $\Delta\lambda c$  (the slope according to the terrain shape). In order to estimate this parameter with higher precision a proximity sensor is used which is situated under the platform. The odometry of the system is based in absolute encoders. Due to this, the positioning error increases when the robot is further displaced. Future research includes using external sensors, like GPRS, to refresh the actual position, experimentation in the field, incorporate a vision system in order to detect objectives, instrumentation of the end effector in order to carry out different kinds of manipulation and the implementation of the presented modeling methodology in other mobile manipulator configurations. Furthermore, Human-robot interfaces will be studied in order to make the teleoperation of the system more intuitive [34].

**Acknowledgments** Authors would like to acknowledge the Centro de Ingeniería y Desarrollo Industrial (CIDESI) for funding this work.

## References

1. [www.qinetiq-na.com/products/unmanned-systems/talon/](http://www.qinetiq-na.com/products/unmanned-systems/talon/), (last visit 8.10.2013)
2. [www.northropgrumman.com/capabilities/remotec](http://www.northropgrumman.com/capabilities/remotec) (last visit 8.10.2013)
3. Will, P., Grossman, D.: An experimental system for computer controlled mechanical assembly. *IEEE Trans. Comput* **24**, 879–888 (1975)
4. Jian-Jun, Z., Ru-Qing, Y., Wei-Jun, Z., Xin-Hua, W., Jun, Q.: Research on Semi-Automatic Bomb Fetching for an EOD Robot. *ARS Advanced Robotics System* (2007)



5. Dongseok, R., Chang-Soon, H., Sungchul, K., Munsang, K., Jae-Bok, S.: Wearable haptic-based multi-modal teleoperation of field mobile manipulator for explosive ordnance disposal. Safety, Security and Rescue Robotics, Workshop, IEEE International (2005)
6. Sungchul, K., Changhyun, C., Jonghwa, L., Dongseok, R., Changwoo, P., Kyung-Chul, S., Munsang, K.: ROBHAZ-DT2 Design and integration of passive double tracked mobile manipulator system for explosive ordnance disposal. In: Proceedings of the IEEE/RSJ International Conference on Intelligent Robots and Systems (IROS) (2003)
7. Yamamoto, Y., Yun, X.: Coordinating locomotion and manipulation of a mobile manipulator. IEEE Transactions on Automatic Control, 6th edn., vol. 39, June (1994)
8. Mazur, A., Szakiel, D.: On path following control of nonholonomic mobile manipulators. Int. J. Appl. Math. Comput. Sci. **19**(4), 561–574 (2009)
9. Bayle, B., Fourquet, J.Y., Renaud, M.: Nonholonomic mobile manipulators: Kinematics, velocities and redundancies. J. Intell. Robot. Syst. **36** (2003)
10. Bayle, B., Fourquet, J.Y., Renaud, M.: Manipulability of wheeled mobile manipulators: Application to motion generation. Int. J. Robot. Res. **22**(708), 565–581 (2003)
11. Krus, P.: Distributed Techniques for Modelling and Simulation of Engineering Systems. Technical Report. Department of Mechanical Engineering Linköping University, Linköping (2000)
12. Wiens, G.I.: Effects of dynamic coupling in mobile robotic systems. In: Proceedings SME Robotics Research World Congress, Gaithersburg MD, pp. 43–57 (1989)
13. Padois, V., Fourquet, J.Y., Chiron, P.: Kinematic and dynamic model-based control of wheeled mobile manipulators: a unified framework for reactive approaches. Robotica **25**(2), 157–173 (2007). doi:[10.1017/S0263574707003360](https://doi.org/10.1017/S0263574707003360)
14. Kang, S., Komoriya, K., Yokoi, K., Koutoku, T., Tanie, K.: Utilization of inertial effect in damping-based posture control of mobile manipulator. In: Proceedings of the 2001 IEEE International Conference on Robotics and Automation, pp. 1277–1282. Seoul (2001)
15. Umeda, Y., Nakamura, D., Mukarami, T., Ohnishi, K.: Hybrid position/force control of a mobile manipulator based on cooperative task sharing. In: Proceedings of the IEEE International Symposium on Industrial Electronics, Bled, Slovenia (1999)
16. Brock, O., Khatib, O., Viji, S.: Task consistent obstacle avoidance and motion behavior for mobile manipulation. In: Proceedings of the International Conference on Robotics and Automation, pp. 388–393. Washington DC (2002)
17. Kang, Y., Li, Z., Dong, Y., Xi, H.: Markovian based fault-tolerant control for wheeled mobile manipulators. IEEE Trans. Control Syst. Technol. **20**(1), 266–276 (2012)
18. Yangmin, L., Yugang, L.: Dynamics and Control for Nonholonomic Mobile Modular Manipulators, Mobile Robotics, Moving Intelligence. InTech (2006)
19. White, G.D., Bhatt, R.M., Krovi, V.N.: Dynamic redundancy resolution in a nonholonomic wheeled mobile manipulators. Robotica J. Camb. Univ. Press. **25**(2), 147–156 (2006)
20. Maza, I., Ollero, A.: Hemero: a matlab-simulink toolbox for robotics. 1st Workshop on Robotics Education and Training, pp. 43–50 (2001)
21. Padois, V., Fourquet, J.Y., Chiron, P., Renaud, M.: On contact transition for nonholonomic mobile manipulators. 9th International Symposium on Experimental Robotics, ISER, pp. 207–216 (2006)
22. Li, Z., Li, J., Kang, Y.: Adaptive robust coordinated control of multiple mobile manipulators interacting with rigid environments. Automatica **46**, 2028–2034 (2010)
23. Li, Z., Yang, C., Tang, Y.: Decentralized adaptive fuzzy control of coordinated multiple mobile manipulators interacting with nonrigid environments. IET Contr. Theor. Appl. **7**(3), 397–410 (2013)
24. Li, Z., Ge, S.S., Ming, A.: Adaptive robust motion/force control of holonomic constrained nonholonomic mobile manipulators. IEEE Trans. Syst. Man Cybernet. B **37**(3), 607–617 (2007)
25. Paul, R.P.: Robot manipulators: mathematics, programming and control. MIT Press, Massachusetts (1981)
26. Zúñiga-Avilés, L.A., Pedraza-Ortega, J.C., Gorrostieta, E., Ramos, J.M.: Analysis of dynamic behavior of an EOD mechatronic unit. In: International Conference on Electronics, Robotics and Automotive Mechanics Conference, CERMA (2009)
27. Zúñiga-Avilés, L.A., Pedraza-Ortega, J.C., Gorrostieta, L., García-Valdovinos, J.M., Ramos, J.M.: Herrera: Modeling and simulation of a mechatronic unit EOD/IEDD. In: International Conference on Methods and Models in Automation and Robotics (2009)
28. Zúñiga-Avilés, L.A., Pedraza, J.C., Gorrostieta, E., Ramos, J.M.: New approach to modeling and simulation methodology for the mechatronic design of IEDD-unmanned wheeled mobile manipulator. In: International Conference on Electronics, Robotics and Automotive Mechanics Conference, CERMA, México, D.F. (2010)
29. Zúñiga-Avilés, L.A., Skodny, T., Pedraza-Ortega, J.C., Gorrostieta, E.: Systematic Analysis of an IEDD unit based in a new methodology for modeling and simulation. J. Adv. Robot. INTECH, Austria **7**, 93–100 (2010)
30. Apostolopoulos, D.: Analytical Configuration of Wheeled Robotic Locomotion. Carnegie Mellon University, Doctoral Thesis, U.S.A. (2001)
31. Skodny, T.: Forward and inverse kinematics of IRb-6 manipulator. Mach. Theory Pergamon Press. Lond. **30**(7), 1039–1056 (1995)
32. National Defense Secretariat: Searching and localization of explosive devices and explosive traps manual, Mexican Industrial Army General Direction. Mexico (2005)
33. Brodie, T.G.: Bombs and bombings: A handbook to protection, security, disposal, and investigation for industry, police and fire Departments. Thomas Publisher, Ltd, Illinois, U.S.A. (2005)
34. Wang, B., Li, Z., Ye, W., Xie, Q.: Development of human-machine interface for teleoperation of a mobile manipulator. Int. J. Contr. Automat. Syst. **10**(6), 1225–1231 (2012)